Chinese Chemical Letters 36 (2025) 109530

Contents lists available at ScienceDirect

Chinese Chemical Letters

journal homepage: www.elsevier.com/locate/cclet

Bistable switch molecule $DPACdCl_4$ showing four physical channels and high phase transition temperature

Ying-Yu Zhang[a,1], Jia-Qi Luo[a,1], Yan Han[a], Wan-Ying Zhang[a,b], Yi Zhang[a], Hai-Feng Lu[a,*], Da-Wei Fu[a,b,*]

[a] Institute for Science and Applications of Molecular Ferroelectrics, Key Laboratory of the Ministry of Education for Advanced Catalysis Materials, Zhejiang Normal University, Jinhua 321004, China
[b] Ordered Matter Science Research Center, Jiangsu Key Laboratory for Science and applications of Molecular Ferroelectrics, Southeast University, Nanjing 211189, China

ARTICLE INFO

Article history:
Received 17 October 2023
Revised 11 December 2023
Accepted 17 January 2024
Available online 23 January 2024

Keywords:
Organic-inorganic hybrid
Phase transition
Crystal
Perovskite
Piezoelectricity

ABSTRACT

Multiple switchable physical channels within one material or device, encompassing optical, electrical, thermal, and mechanical pathways, can enable multifunctionality in mechanical-thermal-opto-electronic applications. Achieving integrated encryption and enhanced performance in storage and sensing presents a formidable challenge in the synthesis and functionality of new materials. In an effort to overcome the complexities associated with these multiple physical functions, this study investigates the large-size crystal of $DPACdCl_4$ (DPA = diisopropylammonium), revealing significant features in rare multi-channel switches. This compound demonstrates the ability to switch between "OFF/0" and "ON/1" states in the mechanical-thermal-opto-electronic channels. Consequently, $DPACdCl_4$ possesses four switchable physical channels, characterized by a higher phase transition temperature of 440.7 K and a competitive piezoelectric coefficient of 46 pC/N. Furthermore, solid-state NMR analysis indicates that thermally activated molecular vibrations significantly contribute to its multifunctional switching capabilities.

The utilization of multiple switchable physical channels, such as optical, electrical, thermal, and mechanical pathways, at the basic device level is a common practice. However, integrating two or more distinct switchable physical channels within a single material can open up new possibilities, leading to a diverse range of applications and even the emergence of novel research fields [1,2].This integration of multiple physical channels within a single device, encompassing thermoelectric, optoelectronic, magneto-optical, mechanical-opto-electronic, and even mechanical-thermal-opto-electronic functionalities, holds the potential to achieve advanced levels of encryption, integration, and multifunctionality [3–5]. Bistable physical channel switches, operating in high-active ON (or 1) and low-active OFF (or 0) states, can be triggered by various environmental stimuli such as light, electric fields, pressure, ambient temperature, and thermal stimulation. This ability enables multiple data exchange and storage [6–12]. Stimuli-responsive, switchable multiple physical channels have transformed into a class of exciting, highly desirable, and controllable intelligent devices [13–18]. However, developing multiple switchable crystalline materials with rich and excellent characteristics remains a significant challenge [3–5]. Recently, crystalline molecular compounds have emerged as competitive and effective complements or successors to traditional inorganic materials in device design and data encryption [19–24]. This shift is attributed to their tunable phase transition freedom, environmentally friendly processing, lightweight properties, and mechanical flexibility. At present, some molecular bistable switching materials and some materials with multiple physical channels at the same time have been studied [25]. Most known molecular switchable materials exhibit low phase transition temperatures, limited physical channels, and weak piezoelectric efficiency, restricting their practical applications [26–31]. To address these challenges, this study focuses on the orientational disorder or twist of diisopropylammonium (DPA) above room temperature, leading to symmetry breaking and bistable structural phase transitions [3,32–36]. In this study, DPA is introduced as a functional unit, balanced with $CdCl_2$ and HCl, forming an unprecedented molecular switch with four physical channels. Notably, this molecular switch demonstrates several distinct features: (1) Four switchable physical channels [7]: The switch exhibits versatility across four

* Corresponding authors at: Institute for Science and Applications of Molecular Ferroelectrics, Key Laboratory of the Ministry of Education for Advanced Catalysis Materials, Zhejiang Normal University, Jinhua 321004, China.
E-mail addresses: luhaifeng@zjnu.edu.cn (H.-F. Lu), dawei@seu.edu.cn (D.-W. Fu).
[1] These authors contributed equally to this work.

https://doi.org/10.1016/j.cclet.2024.109530
1001-8417/

different physical channels. (2) High phase transition temperature: The large-size crystal $DPACdCl_4$ possesses the highest phase transition temperature (440.7 K). (3) Competitive piezoelectric coefficient (d_{33}): The piezoelectric coefficient d_{33} reaches 46 pC/N at room temperature, which represent one of the highest values in molecule-based piezoelectrics [36,37]. (4) Non-centrosymmetrical structures: Both bistates feature non-centrosymmetrical structures, showcasing pyroelectric and nonlinear optical activity. Pyroelectricity can switch from 8.1 μC/cm^2 (On state) to 1.7 μC/cm^2 (OFF state) [38–41]. Additionally, the switching of second-harmonic generation (SHG) effects is completely reversible and recoverable, transitioning between strong and weak states. (5) Mechanism studies: Analyses involving temperature-variable crystal structure, solid-state NMR, and IR spectroscopy have been conducted to understand the origin of the phase transition and switching, highlighting an efficient method for studying these processes. This breakthrough opens avenues for designing and obtaining multiple channel molecular switches, a characteristic previously unseen in molecular materials. Furthermore, solid-state NMR mechanism studies reveal that both the freezing of thermally activated molecular vibrations and atomic displacements significantly contribute to its multi-channel switching. These attributes pave the way for the functional integration of optical-electrical-thermal-mechanical features within a single device. The functional design and regulation of molecular-based phase change materials represent a highly promising research area [42–45]. This study serves as a reliable reference model for future research endeavors in this field [45–50].

Synthesis and crystal growth: All reagents and solvents in the synthesis were of reagent grade and used without further purification. Compound $DPACdCl_4$ was synthesized by employing the solvothermal reaction: diisopropylamine (2 mmol, 0.202 g) and HCl (2 mmol, 0.200 g) were added into 10.0 mL H_2O under constant stirring. $CdCl_2$ (2 mmol, 0.496 g) was dissolved in 10 mL dilute hydrochloric acid solution. Then, the above two solutions were mixed to obtain a mixed solution. Colorless block monophasic crystals of $DPACdCl_4$ suitable for X-ray diffraction were obtained in 58 % yield (based on $CdCl_2$) *via* slowly evaporating the mixed solution at room temperature over two weeks [45,47–52]. Large-size crystals were obtained by cooling the saturated aqueous solution with a relatively low velocity of 0.1 K/day (Fig. S8 in Supporting information). Crystal data measured by Bruker·D8·VENTURE single crystal instrument: Phase I ($T = 298$ K): $C_{12}H_{31}N_2Cl_4Cd$, colorless block, $0.3 \times 0.3 \times 0.2$ mm, $M_r = 457.59$, Monoclinic, $C2$, $a = 28.9429(2)$ Å, $b = 12.2653(2)$ Å, $c = 13.9657(2)$ Å, $\beta = 118.069(3)^o$, $V = 4374.6(7)$ Å^3, $Z = 8$, $D_{calcd.} = 1.390$ mg/m^3. Phase II ($T = 445$ K): $C_{12}H_{31}N_2Cl_4Cd$, colorless block, $0.3 \times 0.3 \times 0.2$ mm, $M_r = 457.59$, Orthorhombic, *Iba*2, $a = 14.443(3)$ Å, $b = 26.445(9)$ Å, $c = 12.355(2)$ Å, $V = 4719(2)$ Å^3, $Z = 8$, $D_{calcd.} = 1.288$ mg/m^3. CCDC 2301559 and 2301560 contain the supplementary crystallographic data for this paper.

DSC thermal anomalies and TG thermal stability: The DSC shows a main endothermic peak at a higher temperature of 440.7 K (phase transition temperature T_c) and a main exothermic peak on cooling at 433 K (Fig. 1a). The sharp shape of these two main peaks and the thermal hysteresis of 7 K reveal a characteristic of first-order phase transition ($\Delta S = \Delta H/T_c = 3.34$ J mol^{-1} K^{-1}) [3,6]. This indicates that the DPA cations are much more disordered or displaced above the T_c than in the LTP (low-temperature phase). TGA measurements show that the loss of cations occurred at 481 K (much higher than the phase transition temperature 440.7 K) (Fig. S7 in Supporting information), these results prove the stability of $DPACdCl_4$ molecule below the measured phase transition temperature ranges (455 K). The high T_c of compound $DPACdCl_4$ is comparable to that of a typical inorganic ceramic $BaTiO_3$ ($T_c = 393$ K) and obviously higher than those of most previously reported molecule-based bistable dielectrics, such as $[(CH_3)_2NH_2]\cdot[Mn(HCOO)_3]$ ($T_c = 187$ K), TGS

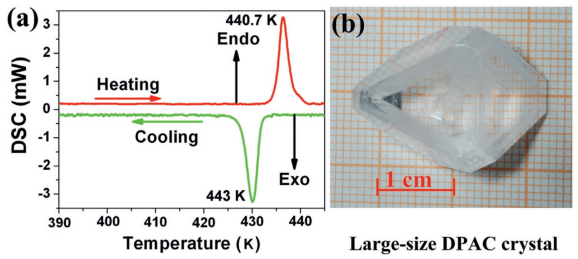

Fig. 1. (a) DSC curves in the heating-cooling cycles, revealing a reversible structural phase transition at 440.7 K for heating and 443 K for cooling. (b) The as-grown crystal with the size of $2.6 \times 2.0 \times 1.9$ cm.

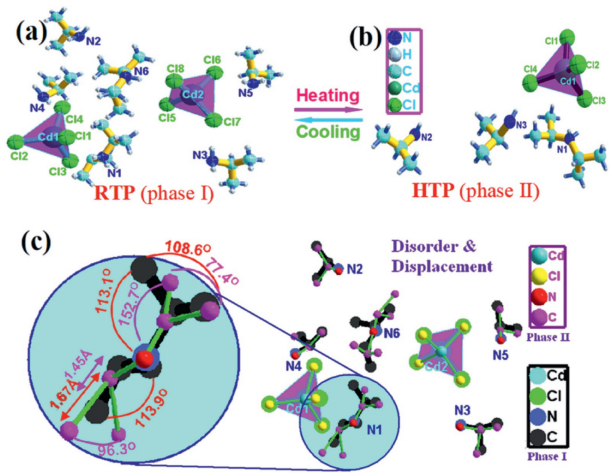

Fig. 2. The asymmetric units. (a) The HTP at 443 K and (b) the RTP at 293 K. (c) The overlap perspective of the two phases. The figure shows the relative rotation and displacement of the cation of high-temperature phase (phase I, black and blue ball) relative to that of room-temperature phase (phase II, pink and red ball). The sites of N and C atoms were refined freely.

($T_c = 322$ K), crown-ether compound series ($T_c = 140$–200 K) and $[NH_2NH_3]\cdot[Mg(HCOO)_3]$ ($T_c = 348$ K) [8,13]. Herein, the compound in this work possesses higher phase transition temperature as shown in Fig. 1a. Meanwhile, the large size crystal image was shown in Fig. 1b.

Bistable switchable crystal structural phase transition: In order to investigate the structural changes and molecular motions of $DPACdCl_4$, the room-temperature (293 K) and the high-temperature (443 K) single crystal structure measurements have been performed [11]. The polar-to-polar (bistability) phase transition has been confirmed by the determination of variable-temperature crystal structures. The room temperature phase (RTP) structure is monoclinic, space group $C2$ (No. 5). The high temperature phase (HTP) structure, measured at 443 K, is orthorhombic and its space group turns into *Iba2* (No. 45). The unit cell parameters of $DPACdCl_4$ at the two different temperatures have been changed abruptly and remarkably, indicating that it displays a reversible first-order phase transition, which matches well with the results of the DSC and SHG measurements (see below). The asymmetric unit of the RTP structure at 293 K contains two and four halves of the protonated DPA cations, and two isolated $CdCl_4^{2-}$ anion (Fig. 2a). The cations and anions stack head-to-tail through N–H···Cl bonds to result in a noteworthy 3-D network structure (Fig. S3a in Supporting information). By comparing the two phases (RTP (phase I) and HTP phase (phase II)), it can be found that the axis lengths and β angle were changed (phase I: space group $C2$, $a = 28.943(1)$ Å, $b = 12.265(3)$ Å, $c = 13.966(3)$ Å, $\beta = 118.069(3)^o$; phase II: space group *Iba2*, $a = 14.443(3)$ Å, $b = 26.445(9)$ Å, $c = 12.355(2)$ Å). This is because the ellipsoid vibration for all atoms are beyond the rea-

sonable range at 440.7 K, and the positions of N atoms and cations were displaced or twisted, which lead to the symmetric elements to be increased, hereby, only one and two halves of the cations and one anion were presented in the asymmetric unit for HTP phase (Fig. 2b). More importantly, the cations shown disordered C–C(N) bond lengths and C–C(N)-C(N) angles range from 77.4 to 132.8, respectively (Fig. 2c), indicating the presence of highly disordered twist motions of the cations (Fig. S3b in Supporting information). Symmetry breaking phenomenon occurs during the transition from the HTP to LTP, a total symmetry decreasing from four symmetry elements to two symmetry elements. Thus, this phase transition may be ferroelastic with an Aizu notion of 2*F*mm2. Spatial symmetric operations change is shown in Fig. S9 (Supporting information). Curie symmetry principle tells us that the space group at ferroeleastic phase should be the sub-space group at the paraelastic phase, *i.e.*, its maximal non-isomorphic sub-groups containing *Cc*, *C*2, *Pba*2, *Pbc*2_1, *Pca*2_1 and *Pcc*2, respectively. Furthermore, spatial symmetric operation numbers decreases from 4 [(1) 1; (2) 2 0, 0, *z*; (3) *a x*, 1/4, *z*; (4) *b* 1/4, *y*, *z*] to 2 [(1) 1; (2) 2 0, 0, *z*] during symmetry breaking process in good agreement with macroscopic symmetry breaking [6,45,48–50]. As the phase transition from LTP to HTP in Fig. 2c, the thermal vibration of the cation becomes more intense after the phase change, resulting in the crystallization of the compound in a centrosymmetric structure. This results in the highly disordered and twisted motion of cations and the Cd-N distances increase or decrease clearly as the temperature rises to the phase transition temperature. The disorder and twist motions of cations contributed the structural phase transition, dielectric, SHG and thermodynamic anomalies.

The SHG switch/channels were thoroughly investigated [7–10]. Both phases exhibit SHG activity, as illustrated in Fig. 3a, demonstrated a sudden enhancement in the relative SHG signal intensity around T_c. This indicates the formation of a non-centrosymmetric to non-centrosymmetric phase change within this temperature range. In the high-temperature phase (HTP), it displays robust SHG activities with intensity approximately 2.5 times larger than that of potassium dihydrogenphosphate (KDP). Consequently, its quadratic coefficient $\chi(2)$ is estimated to be 1.34 pm/V (where $\chi(2)$KDP ≈ 0.39 pm/V), surpassing other non-liner optics (NLO) switches such as photochromic crystals [14] and other metal-organic frameworks

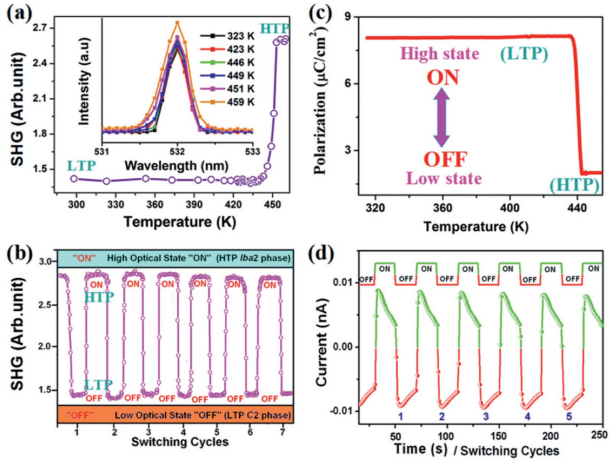

Fig. 3. (a) SHG characterization for the structural phase transition. The inset shows the wavelength dependence of SHG intensity at different temperatures. (b) The completely reversible and recoverable switching of NLO effects with the resumption of SHG ON/OFF cycles. (c) Temperature dependence of spontaneous polarization by integrating the pyroelectric current along the crystallographic *b*-axis for the structural phase transition. (d) Pyroelectric current measured at room temperature when the infrared laser changes between ON and OFF states, showing the bistable switching effect.

[13]. Conversely, cooling below the T_c of 440 K results in a relatively weak SHG signal with a stepped shape change, defining the low-temperature phase as the SHG low-active state. These low-active (LTP) and high-active (HTP) SHG states can be switched by warming or cooling.

The reversibility of $DPACdCl_4$ was confirmed through NLO switching cycles, cyclically cooling and heating the crystal sample. Fig. 3b shows the gratifying results: its SHG activities at the high-NLO state can be recovered after several cycles without any signal attenuation, confirming $DPACdCl_4$'s superior stability compared to other switching systems, including photochromic ones. Its higher sensitivity SHG bistability, with strong high-/low-active contrast, renders it invaluable for applications in optical switches, especially in sensing, switchable devices, and data storage.

Pyroelectric bistability (thermoelectric switch): The pyroelectric bistable switchable channels were also confirmed by the pyroelectric measurement, and pyroelectric bistable switchable effect showing two level states was observed obviously. The single crystal structure analysis and SHG measurement reveal that $DPACdCl_4$ is polar structure below and above the T_c (polar to polar transition). According to the Landau phenomenological theory, the SHG, dielectric response and pyroelectricity in the vicinity of T_c are essentially associated with the appearance of P_s. The spontaneous polarization integrated from pyroelectric current along the *b*-axis in a heatling/cooling process as a function of temperature is shown in Fig. 3c. As expected, P_s reaches 8.1 μC/cm^2 in LTP, hence, LTP represents a high-active state. P_s begins to gradually decrease to 1.7 μC/cm^2 at around T_c, it means the presence of switching low-active state of HTP. The sudden decrease of P_s further confirms the uncontinuous character of the dipolar transition showing high and low states. Such bistable pyroelectric response is very interesting to pyroelectric infrared sensor and thermoelectric data storage.

Moreover, to investigate the reversible photoelectric switchable effect around room temperature, pyroelectric current was measured by turning an infrared laser (1064 nm) on or off through the Chynoweth technique. This method periodically heated the crystal samples (sliced along the polar axis) using a rectangular wave (Fig. 3d). During the heating process with the infrared laser on, a negative current peak of approximately 0.01 nA was observed due to the sudden increase in sample temperature. Subsequently, the current declined to zero as the temperature stabilized. During the cooling process with the infrared laser off, a symmetrical positive current peak of the same value was observed due to the sudden temperature decrease. A pair of switching current effects, between each ON/OFF and OFF/ON transition, emerged in the opposite direction, consistent with the dipolar change induced by the temperature increase and decrease. Notably, the current peaks during ON and OFF processes were approximately symmetrical, indicating negligible thermal stimulation current. These observations ruled out interference from other mechanisms, such as trapped charge or electrets, confirming that the observed current is unequivocally the pyroelectric current. In the laser-induced effect, positive and negative pyroelectric current peaks alternated, corresponding to the ON (LTP) and OFF (HTP) states, respectively.

In this study, the piezoelectric coefficient d_{33} was measured using a *quasi*-static method and was found to reach 46 pC/N at room temperature, which is notably higher than most molecule-based piezoelectric materials (Fig. S10 in Supporting information). In detail, the topographic image of the crystal surface shown in Figs. 4a and b is 3D topographic image of the crystal surface. Moreover, the phase and amplitude hysteresis loops at two different positions in the crystal surface showing the bistable switchable effect as illustrated in Figs. 4c and d. This measurement was conducted using single crystal samples along the polar axis (Fig. 4e). Generally, the d_{33} coefficient of molecule-based and various inorganic or molecule-based piezoelectric materials fall bellows 40 pC/N

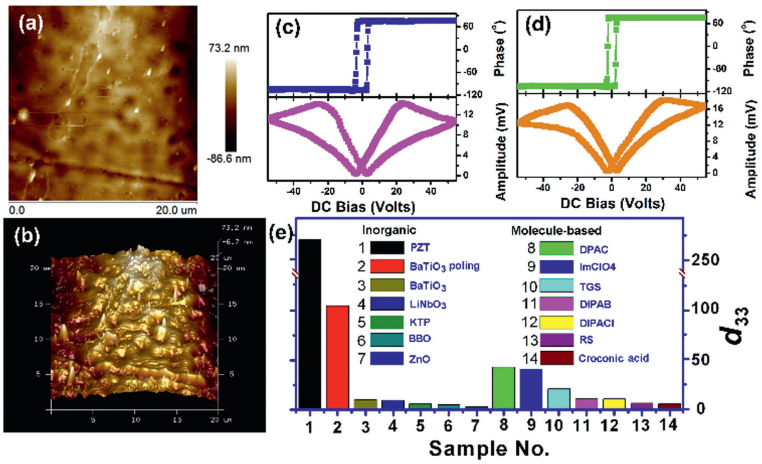

Fig. 4. (a) The topographic image of the crystal surface. (b) 3D topographic image of the crystal surface. (c, d) phase and amplitude hysteresis loops at two different positions in the crystal surface showing the bistable switchable effect. (e) The histogram of piezoelectric coefficient of a series of inorganic and molecule-based piezoelectric material. The d_{33} piezoelectric coefficient reaches 46 pC/N.

(Fig. 4e). For instance, the piezoelectric coefficients d_{33} of TGS, PVDF, DIPAB, KTP, and $LiNbO_3$ are 35, 31, 11, 10, and 8 pC/N, respectively [3–12]. The organic Im-ClO_4 piezoelectric material shows a d_{33} of 41 pC/N, synthesized by our group [3,6,7]. Another high value, 45 pC/N, reported by Xiong's group, pertains to a high-pressure electrical material [7,36–38]. An inverse piezoelectric effect was measured by applying a voltage of 1000 V, revealing an observable electrostrictive effect of 38 nm (Fig. S5 in Supporting information). Consequently, the calculated piezoelectric coefficient at LTP is 38 pC/N, which is consistent with the experimental values. In contrast, the inverse piezoelectric effect at HTP was calculated to be nearly zero. Additionally, piezoresponse force microscopy (PFM) was employed to measure the local piezoelectric response at the nanoscale on crystal samples (Fig. 4). This method has recently proven to be highly sensitive for piezo- and ferroelectric measurements on ferroelectric crystalline materials [3,6]. In spectroscopic PFM, hysteresis loop measurements were conducted by applying voltage pulses (V_{dc}) of variable height (up to 100 V) at different locations on the crystalline surface. The crystalline surface is approximately perpendicular to the *b*-axis of $DPACdCl_4$ crystal [45,48,49]. The amplitude of the piezoresponse is proportional to converse d_{33}. Switching PFM experiments were performed, with DC voltage applied on top of the AC voltage to switch the polarization. This resulted in characteristic hysteresis and butterfly loops (Figs. 4c and d). These results are in agreement with those observed in typical molecular ferroelectrics such as triglycine sulfate (TGS), potassium sodium tartrate tetrahydrate (RS), and diisopropylamium bromide (DIPAB) [3,45], where both amplitude and phase as a function of V_{dc} display typical hysteresis loops and butterfly curves. Notably, the butterfly-like amplitude shape indicates bistable switching, aligning with macroscopic pyroelectricity and nonlinear characteristic (SHG) measurements. The high symmetric structural phase transition (from 2 to *mm*2 point group) causes significant changes in surface energy, resulting in substantial piezoelectric strain. These findings further affirm the electrical switchable bistability of this molecular crystal. It suggests that this sample might be one of the potential molecular piezoelectric switchable materials. The piezoelectric states can be switched by warming/cooling or applying an electric field, showcasing promising applications in the realm of mechanically switchable materials.

Dielectric bistability: Structural phase transitions involving molecular motions often lead to significant anomalies in dielectric and other physical properties. In the case of $DPACdCl_4$, molecular and atomic dipole motion, including displacement, twist, and disorder, plays a crucial role in its prominent dielectric response

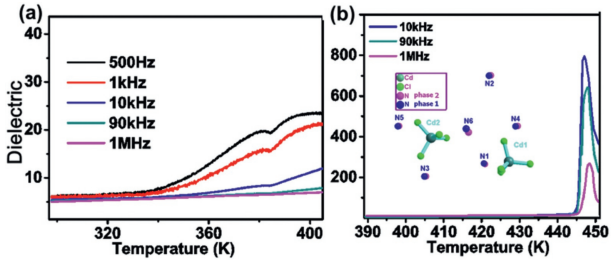

Fig. 5. (a, b) Dielectric responses at various frequencies (500 Hz, 1 kHz, 10 kHz, 90 kHz and 1 MHz) with variation of the temperature are presented upon the heating process. Inset of (b) the displacement of phase I and phase II for 293 K and 443 K.

[3,7–10]. Fig. 5a illustrates the real part of the temperature-dependent dielectric constant of $DPACdCl_4$ along the polar axis at various frequencies. Notably, a strong anomaly and a sharp peak are observed around the T_c. At a low frequency, the dielectric temperature dependence indicates a continuous bistable phase transition. The peak maxima of ε' remain nearly unchanged at different frequencies, signifying the absence of relaxation within the measured frequency range. However, the values of ε' increase with decreasing frequency. The sharp peak and robust dielectric anomalies are attributed to the highly mobile motion of $DPACdCl_4$ cations, as confirmed by variable-temperature structural analysis. Low-frequency dielectric properties are more sensitive to molecular motion, and the sharp peak around T_c at low frequencies is ascribed to the displacive twist and disorder of the cations. This implies that $DPACdCl_4$ does not exhibit typical displacive or order-disorder type dielectric behavior. Additionally, there is a small permittivity increase in the temperature range of 350–400 K, corresponding to a slight twist of cations, consistent with the single crystal structural analysis (Fig. 5a and Fig. S4 in Supporting information). The disorder transition processes lead to the high values of ε'. The gradual increase in angular oscillations provides a means to tune ε' (Fig. 5b), and the phase transition itself enables the switching of the dielectric constant [50–52].

Mechanism discussion (variable-temperature solid-state NMR and IR): To provide an insight into the molecular motion and bistable switching mechanism, the nature of its switchable effects and structure change were further studied. Therefore, we performed the variable-temperature solid-state NMR (Fig. 6) and IR (Fig. S11 in Supporting information) investigate the motion of $DPACdCl_4$. The freezing of thermally activated molecu-

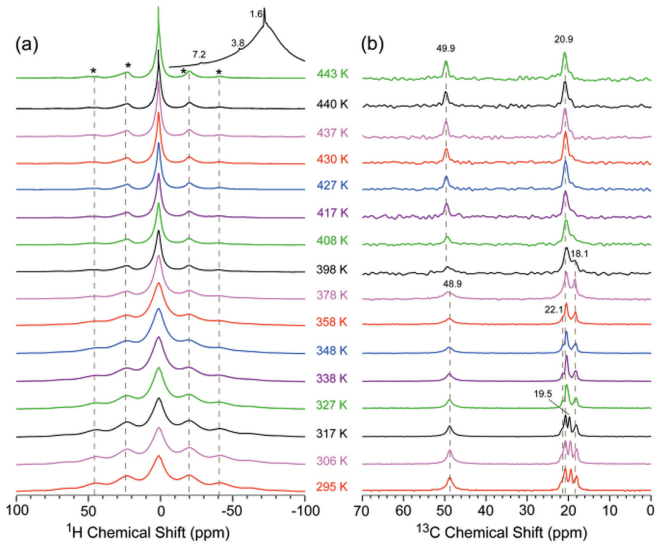

Fig. 6. Variable-temperature (a) ^{1}H MAS and (b) ^{13}C CP/MAS NMR spectra of $DPACdCl_4$. Asterisks denote spinning sidebands.

lar vibrations and atomic displacements are greatly contributive to its optical-electrical-thermal-mechanical multi-functional four-channel switching.

Fig. 6a shows the ^{1}H MAS NMR spectra of $DPACdCl_4$ ac-quired at variable temperature. A broad peak centered at 1.6 ppm along with its spinning sidebands can be clearly observable at the temperature range of 295–358 K (Fig. 6a). Broad line width in ^{1}H MAS NMR spectra is probably resulted from the presence of strong ^{1}H-^{1}H homo-nuclear dipole interaction, indicating the rigidity of DPA cation below 358 K. As temperature varies in range of 378–408 K, the predominant peak line width as well as the relative intensity of spinning sidebands in ^{1}H MAS NMR spectra decreases gradually, suggesting the acceleration of twist motion of DPA upon increasing the temperature. No significant variation can be discerned at the temperature range of 408–437 K. As temperature approaches to T_c, three additional sharp signals arising from DPA cation can be clearly resolved. It can be revealed that parts of DPA cation performing twist motion become highly mobile at HTP [53,54].

Fig. 6b shows the variable temperature ^{13}C CP/MAS NMR spectra. At the temperature range of 295–378 K, the signal at 48.9 ppm is unambiguously assigned to CH site of the DPA cation. Additionally, the resonances in range of 18.1–22.1 ppm can be ascribed to the terminal methyl groups. The chemical shifts distribution of the methyl group is resulted from the asymmetric unit of DPA cation at LTP. Further increasing the temperature to 408 K, the presence of twist motion of DPA induces the asymmetry breaking of the independent crystallographic methyl groups. As a result, only one type of methyl signal can be distinguished at temperature above 408 K.

As temperature increases to 398 K, the resonance at 48.9 ppm due to CH site is significantly shifted to 49.9 ppm, indicating the structural variation of DPA cation in HTP in comparison with RTP, which is in good consistence with the single-crystal XRD data. Additionally, DIPSHIFT experiments are further employed to quantitatively characterize the molecular motions of the cation at various temperatures. In the DIPSHIFT experiments, the simulated one-bond C–H coupling strength relative to rigid limit (23.9 kHz), namely order parameter, can directly manifest the regional molecular motion. Fig. S6 (Supporting information) shows the temperature-dependent order parameters for CH group of cation [55]. As manifested in Fig. S6, the determined order parameter for CH group generally approaches the rigid limit at the temperature range of 295–358 K, confirming the rigidity of cation below 358 K, which agrees well with the experimental results from ^{1}H VT MAS NMR. Moreover, the progressive increase of twist motion amplitude of cation upon increasing the temperature to 443 K, can be further evidenced from the DIPSHIFT analysis (Fig. S6).

Based on the variable-temperature solid-state NMR, the dynamic behavior of cation can be summarized as following: (1) DPA is considerably rigid below 358 K; (2) DPA cation performs twist motion at the temperature range of 378–443 K. It should be noteworthy that parts of DPA become highly mobile above phase transition temperature (440 K), which is consistent with the single crystal XRD and dielectric data discussed above. The freezing of thermally activated molecular vibrations and atomic displacements are greatly contributive to its optical-electrical-thermal-mechanical multi-channel switching [56–58].

In summary, the large-sized $DPACdCl_4$ crystal emerges as an exemplary high-temperature material ($T_c = 440.7$ K) featuring multiple switchable functions across electrical, optical, thermal, and mechanical channels. This crystal exhibits synchronous functionality, making it an ideal candidate for diverse applications. The crystal incorporates high-active "ON or 1" and low-active "OFF or 0" bistable switches encompassing optical, electrical, thermal, and mechanical channels. Environmental stimuli such as light, electric fields, ambient temperature, and pressure can trigger the switching of these channels. The exceptional physical properties of this crystal stem from the remarkably mobile motions of DPA cations, as observed through temperature-variable crystal analyses (phase transition denoted as *mm2F2* in Aizu notation), solid-state NMR, and infrared spectroscopy. Mechanistic studies utilizing solid-state NMR techniques elucidate that both the freezing of thermally activated molecular vibrations and atomic displacements significantly contribute to its multi-channel switching behavior. This research serves as a catalyst for exploring novel molecule-based materials with multiple bistable switches, boasting an increased number of physical channels and a substantial piezoelectric coefficient. These advancements pave the way for their integration into multifunctional intelligent devices, marking a significant stride in the field of materials science.

Declaration of competing interest

The authors declare that they have no known competing financial interests or personal relationships that could have appeared to influence the work reported in this paper.

Acknowledgments

This work was financial supported by National Natural Science Foundation of China (No. 52303256), Natural Science Foundation of Zhejiang Province (No. LQ23B040004) and Jinhua Industrial Major Project (No. 2022-1-043).

Supplementary materials

CCDC 2301559 and 2301560 contain the supplementary crystallographic data for this paper. These data can be obtained free of charge from The Cambridge Crystallographic Data Centre via www.ccdc.cam.ac. uk/data_request/cif.

Supplementary material associated with this article can be found, in the online version, at doi:10.1016/j.cclet.2024.109530.

References

[1] M. Liu, Z.Y. Zhou, T.X. Nan, et al., Adv. Mater. 25 (2013) 1435–1439.
[2] B.B. Mukherjee, S.K. Batabyal, A.J. Pal, Adv. Mater. 19 (2007) 717–722.
[3] D.W. Fu, H.L. Cai, Y. Liu, et al., Science 339 (2013) 425–428.
[4] Y. Zhang, H.Y. Ye, H.L. Cai, et al., Adv. Mater. 26 (2014) 4515–4520.
[5] W. Li, A. Thirumurugan, P.T. Barton, et al., J. Am. Chem. Soc. 136 (2014) 7801–7804.

[6] A. Piecha-Bisiorek, A. Bialonska, R. Jakubas, et al., Adv. Mater. 27 (2015) 5023–5027.
[7] Y. Zhang, H.Y. Ye, D.W. Fu, et al., Angew. Chem. Int. Ed. 53 (2014) 2114–2118.
[8] D.Y. Wang, D.Z. Zhang, P. Li, et al., Nano-Micro Lett. 13 (2021) 57.
[9] J. Long, J. Rouquette, J.M. Thibaud, et al., Angew. Chem. Int. Ed. 54 (2015) 2236–2240.
[10] S. Horiuchi, Y. Tokunaga, G. Giovannetti, et al., Nature 463 (2010) 789–792.
[11] H. Xu, R. Chen, Q. Sun, et al., Chem. Soc. Rev. 43 (2014) 3259–3302.
[12] S. Horiuchi, R. Kumai, Y. Tokunaga, et al., J. Am. Chem. Soc. 130 (2008) 13382–13391.
[13] H.Y. Ye, S.H. Li, Y. Zhang, et al., J. Am. Chem. Soc. 136 (2014) 10033–10040.
[14] A. Katrusiak, M. Szafranski, J. Am. Chem. Soc. 128 (2006) 15775–15785.
[15] P. Serra-Crespo, M.A. Veen, E. Gobechiya, et al., J. Am. Chem. Soc. 134 (2012) 8314–8317.
[16] J. Boixel, V. Guerchais, H.L. Bozec, et al., J. Am. Chem. Soc. 136 (2014) 5367–5375.
[17] X. Dong, J. Liang, Z. Xu, et al., Chin. Chem. Lett. 35 (2024) 108708.
[18] X. Zhang, Y. Yao, L. Liang, et al., Angew. Chem. Int. Ed. 61 (2022) e202205939.
[19] G. Teri, Q.Q. Jia, H.F. Ni, et al., Dalton Trans. 52 (2023) 1074–1081.
[20] Y. Zhou, Y. Li, Q. Ding, et al., Chin. Chem. Lett. 32 (2021) 263–265.
[21] L.X. Zhang, L.Y. Mei, K.Y. Wang, et al., Nano-Micro Lett. 15 (2023) 177.
[22] D.X. Liu, H.L. Zhu, W.X. Zhang, et al., Angew. Chem. Int. Ed. 62 (2023) e202218902.
[23] M.M. Lun, J.Q. Luo, Z.X. Zhang, et al., Chem. Eng. J. 475 (2023) 145969.
[24] Y.Y. Yu, P.Z. Huang, Y.Z. Wang, et al., Chin. Chem. Lett. 32 (2021) 3558–3561.
[25] R.G. Xiong, S.Q. Lu, Z.X. Zhang, et al., Angew. Chem. Int. Ed. 59 (2020) 9574–9578.
[26] J.Y. Li, T. Zhang, M.M. Lun, et al., Small 19 (2023) 2301364.
[27] M.M. Lun, C.Y. Su, J. Li, et al., Small 19 (2023) 2303127.
[28] K. Ding, H.S. Ye, C.Y. Su, et al., Nat. Commun. 14 (2023) 2863.
[29] M.M. Lun, H.F. Ni, Z.X. Zhang, et al., Angew. Chem. Int. Ed. 63 (2024) e202313590.
[30] G. Teri, Q.Q. Jia, Q. Guo, et al., Sci. China Mater. 66 (2023) 3687–3695.
[31] H.F. Ni, L.K. Ye, P.C. Zhuge, et al., Chem. Sci. 14 (2023) 1781–1786.
[32] D.Y. Fu, Y.L. Ma, C.Y. Su, et al., J. Mater. Chem. C 11 (2023) 11492–11499.
[33] J.Q. Wang, G. Teri, H.F. Ni, et al., Inorg. Chem. Front. 10 (2023) 3860–3866.
[34] G. Teri, H.F. Ni, Q.F. Luo, et al., Mater. Chem. Front. 7 (2023) 2235–2240.
[35] L.P. Miao, N. Ding, N. Wang, et al., Nat. Mater. 21 (2022) 1158–1164.
[36] Y.M. You, W.Q. Liao, D.W. Zhao, et al., Science 357 (2017) 306–309.
[37] H.Y. Ye, Y.Y. Tang, P.F. Li, et al., Science 361 (2018) 151–155.
[38] H.Y. Zhang, H.H. Jiang, Y. Zhang, et al., Angew. Chem. Int. Ed. 61 (2022) e202200135.
[39] T. Zhang, K. Xu, J. Li, et al., Natl. Sci. Rev. 10 (2023) nwac240.
[40] N. Zhang, W.C. Sun, Y. Zhang, et al., Nat. Commun. 14 (2023) 5854.
[41] Y.Y. Fan, S.Q. Deng, T.Y. Li, et al., Chin. Chem. Lett. 34 (2023) 107796.
[42] H. Peng, Z.K. Xu, Y. Du, et al., Angew. Chem. Int. Ed. 62 (2023) e20230673.
[43] J.C. Liu, Y.H. Ai, Q. Liu, et al., Adv. Mater. 35 (2023) 2302436.
[44] H. Peng, Q. Liu, Y. Liu, et al., Chin. Chem. Lett. 34 (2023) 107980.
[45] M. Rok, P. Starynowicz, A. Ciżman, et al., Inorg. Chem. 59 (2020) 11986–11994.
[46] B. Gao, H. Qi, H. Liu, et al., Chin. Chem. Lett. 35 (2024) 108598.
[47] S.A. Wolf, D.D. Awschalom, D.D. Buhrman, et al., Science 294 (2001) 1488–1495.
[48] M. Mączka, J.-K. Zaręba, A. Gągor, et al., Chem. Mater. 33 (2021) 2331–2342.
[49] K. Mencel, V. Kinzhybalo, R. Jakubas, et al., Chem. Mater. 33 (2021) 8591–8601.
[50] Y.J. Zhao, X. Yin, P.W. Li, et al., Nano-Micro Lett. 15 (2023) 187.
[51] M. Szafranski, A. Katrusiak, K. Stahl, et al., J. Mater. Chem. A 9 (2021) 10769–10779.
[52] M. Mączka, A. Nowok, J.K. Zaręba, et al., ACS Appl. Mater. Interface 14 (2022) 1460–1471.
[53] Q.Q. Jia, T. Shao, L. Tong, et al., Chin. Chem. Lett. 34 (2023) 107539.
[54] Q.Q. Jia, H.F. Lu, J.Q. Luo, et al., Small 20 (2024) 2306989.
[55] T. Yang, Y. Liu, L. Hua, et al., Chin. Chem. Lett. 35 (2024) 108707.
[56] S.N. Du, D. Su, Z.Y. Ruan, et al., Angew. Chem. Int. Ed. 61 (2022) e202204700.
[57] M. Mączka, J.K. Zaręba, A. Gągor, et al., Chem. Mater. 33 (2021) 2331–2342.
[58] J.J. Liang, S.J. Wang, Z. Luo, et al., Nano-Micro Lett. 15 (2023) 5.